(12)

FC

SYSTEMS, SCIENCE AND SOFTWARE

SSS-R-76-2937

COMPARISON OF THEORETICAL AND OBSERVED BODY AND SURFACE WAVES FOR KASSERI, AN EXPLOSION AT NTS

T. C. Bache
T. G. Barker
N. Rimer
J. M. Savino

Topical Report

Sponsored by
Advanced Research Projects Agency
ARPA Order No. 2551

This research was supported by the Advanced Research Projects Agency of the Department of Defense and was monitored by AFTAC/VSC, Patrick AFB, FL 32929, under Contract No. F08606-75-C-0045.

May 1976

P. O. BOX 1620, LA JOLLA, CALIFORNIA 92038, TELEPHONE (714) 453-0060

AFTAC Project Authorization No. VELA T/6712/B/ETR

Program Code No. 6F10

Effective Date of Contract: May 1, 1975

Contract No. F08606-75-C-0045

Principal Investigator and Phone No.
Dr. John M. Savino, (714) 453-0060, Ext. 455

Project Scientist and Phone No.
Dr. Ralph W. Alewine, III, (703) 325-8484

S^3 Project No. 11014

UNCLASSIFIED

SECURITY CLASSIFICATION OF THIS PAGE (When Data Entered)

REPORT DOCUMENTATION PAGE

READ INSTRUCTIONS BEFORE COMPLETING FORM

1. REPORT NUMBER	2. GOVT ACCESSION NO.
3. RECIPIENT'S CATALOG NUMBER	
4. TITLE (and Subtitle) COMPARISON OF THEORETICAL AND OBSERVED BODY AND SURFACE WAVES FOR KASSERI, AN EXPLOSION AT NTS	5. TYPE OF REPORT & PERIOD COVERED Topical Report
6. PERFORMING ORG. REPORT NUMBER SSS-R-76-2937	
7. AUTHOR(s) T. C. Bache, T. G. Barker, N. Rimer and J. M. Savino	8. CONTRACT OR GRANT NUMBER(s) F08606-75-C-0045
9. PERFORMING ORGANIZATION NAME AND ADDRESS Systems, Science and Software P. O. Box 1620 La Jolla, California 92038	10. PROGRAM ELEMENT, PROJECT, TASK AREA & WORK UNIT NUMBERS Program Code No. 6F10 ARPA Order No. 2551
11. CONTROLLING OFFICE NAME AND ADDRESS VELA Seismological Center 312 Montgomery Street Alexandria, Virginia 22314	12. REPORT DATE May 1976
	13. NUMBER OF PAGES 44
14. MONITORING AGENCY NAME & ADDRESS (if different from Controlling Office)	15. SECURITY CLASS. (of this report) Unclassified
	15a. DECLASSIFICATION/DOWNGRADING SCHEDULE

16. DISTRIBUTION STATEMENT (of this Report)

Approved for public release; distribution unlimited.

17. DISTRIBUTION STATEMENT (of the abstract entered in Block 20, if different from Report)

18. SUPPLEMENTARY NOTES

19. KEY WORDS (Continue on reverse side if necessary and identify by block number)

Explosion Seismology
Explosion Source Calculations
KASSERI Explosion
Seismic Coupling
Yield Estimates
Teleseismic Ground Motion
Earth Structure

20. ABSTRACT (Continue on reverse side if necessary and identify by block number)

This report presents the results of a theoretical calculation of the teleseismic body and surface waves for the NTS KASSERI explosion, and a detailed comparison of the synthetic seismograms with those recorded at stations of the Special Data Collection System (SDCS). This study is a comprehensive analysis of the KASSERI event including modeling of the close-in nonlinear ground motion produced by the explosion, propagation of the resulting seismic waves through the earth and computation of synthetic seismograms at designated teleseismic stations.

DD FORM 1 JAN 73 1473 EDITION OF 1 NOV 65 IS OBSOLETE

UNCLASSIFIED

SECURITY CLASSIFICATION OF THIS PAGE (When Data Entered)

388 507

TABLE OF CONTENTS

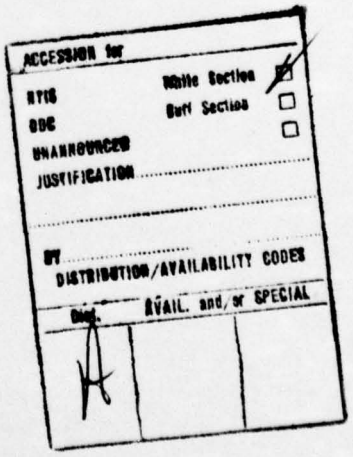

I. INTRODUCTION

This report presents the results of a theoretical calculation of the teleseismic body and surface waves for the underground explosion, KASSERI, and a detailed comparison of the synthetic seismograms with those recorded at stations of the Special Data Collection System (SDCS). A similar exercise was previously carried out for the event, MAST, and was reported by Barker, et al., (1976). For all comparisons we show the results for both MAST and KASSERI.

We have carried out a comprehensive analysis of both MAST and KASSERI using computer modeling of the close-in nonlinear ground motion produced by the explosion, propagation of the resulting seismic wave through the earth and computation of synthetic seismograms at designated teleseismic stations. One of the important questions addressed by this exercise is: What pre-shot measurements of the near-source medium are required in order to predict the amplitude of the seismic signal to within some specified range? This question is kept in mind throughout.

Fundamental to the prediction is the calculation of the explosion reduced displacement potential (RDP) which represents the source coupling into elastic waves. This is the subject of Section II. An important material property for which good data are not available for the KASSERI emplacement material is rock strength. A number of calculations were carried out to determine the effect of plausible variations in strength for the KASSERI tuff. The results of these source calculations are discussed in Section II.

The computation of synthetic teleseismic seismograms and the comparison to observations for both MAST and KASSERI are discussed in Section III. In our MAST report (Barker, et al., 1976) we showed results for a number of earth models. The best of those models was selected for the synthetic

seismograms shown here. The only variation in travel path parameters in the seismograms presented is in the attenuation factor (T/Q) which is taken to be 0.95 and 1.05. The results are not very sensitive to variations on this scale.

We return to the question of the effect of imprecision in material strength estimates in Section 3.4. In this section short period body wave synthetics are computed for the range of source functions discussed in Section II. Study of these seismograms and comparison to the observations allows selection of the source function most appropriate for KASSERI.

A vexatious problem is the specification of the seismometer instrument response that is appropriate for determining ground motion amplitude from observations and for computing comparable synthetics. The amplitudes given in the SDCS Event Reports appear to be based on nominal response curves which differ significantly from the individual station calibration data provided by the Project Officer. Unfortunately, the "apparent ground motion" (seismogram amplitude corrected for instrument response at the apparent period of the cycle measured) is dependent on the shape of the instrument response curve. Therefore, accurate calibration data are imperative if very precise comparison of theoretical and actual ground motion is to be made. In Appendix A we discuss in some detail the awkward fact that the relation between "apparent ground motion" and actual ground motion is dependent on the instrument characteristics even among a class of short period instruments with superficially similar response.

The theoretical and observed short and long period seismograms are compared with respect to amplitude and waveform. The most important result is that the scaling between the synthetic KASSERI and MAST seismograms closely matches the scaling observed. This is important because the body and

surface waves sample different portions of the source spectrum and are sensitive to different properties of the source medium. The agreement at individual stations is well within a factor of two in amplitude nearly everywhere and could be improved with more refined travel path models.

II. CALCULATION OF THE EQUIVALENT ELASTIC SOURCE

Coupling of the explosive energy into elastic waves was computed using the one-dimensional (spherically symmetric) finite difference code, SKIPPER. Description of the technique and the constitutive models may be found in Cherry, et al., (1975).

KASSERI was detonated in ash flow tuff at Area 20, Pahute Mesa. The working point was well below the water table. Standard measurements for density, grain density, overburden density, water content, saturation and P wave velocity were available. It should be noted that the P wave velocity was not measured but was estimated from events in similar media.

No material strength data were available. Therefore, we were forced to estimate the material strength from other information. A study of the effect of plausible strength variations on the seismic signal was carried out as part of the KASSERI investigation and will be discussed.

The equation of state table (pressure as a function of specific volume and specific internal energy) for the saturated tuff was generated using the TAMEOS scheme (Riney, et al., 1972). In this scheme grain density tuff is mixed with the appropriate amount of water, assuming pressure equilibrium between the mixture and its components. From the bulk modulus (K) obtained from the TAMEOS table at the overburden pressure and P wave velocity (α), the shear modulus is calculated from $\rho\alpha^2 = K + 4\mu/3$. The hydrostatic overburden pressure is obtained from the given depth of burial and overburden density.

All calculations used an effective stress law to account for the effect of pore fluid pressure on the stress state. The material was assumed to fail in tension; that is,

a tension failure model was invoked if any principle stress became tensile.

Since no data were available on the shear strength of the KASSERI tuff or similar materials in Pahute Mesa, a series of calculations were made in which the material strength was varied. All other material properties required for the calculation (bulk density, grain density, percent water by weight, percent air-filled voids, P wave velocity, overburden pressure, bulk modulus of overburden, shear modulus) were held fixed at the given values.

Previous calculations for Pahute Mesa rhyolite (Cherry, et al., 1975; Barker, et al., 1976) used a laboratory determined failure envelope for granite. Taking this as a starting point, we then perturbed the failure envelope to values that might be appropriate for the almost certainly weaker tuff. The parameters controlling the failure envelope are summarized in Table 1 for the four calculations completed. The parameters in the table are defined as follows:

$$Y(P,e) = \left(1 - \frac{e}{e_m}\right)\left[Y_0 + Y_m \frac{\bar{P}}{\bar{P}_m}\left(2 - \frac{\bar{P}}{\bar{P}_m}\right)\right], \quad \bar{P} < P_m, \; e < e_m,$$

$$= \left(1 - \frac{e}{e_m}\right)\left(Y_0 + Y_m\right), \quad \bar{P} \geq \bar{P}_m, \; e < e_m,$$

$$= 0, \quad e \geq e_m,$$

$$\bar{P} = P - \frac{1}{2}\sqrt{\frac{J_3'}{2}}$$

where J_3' is the third deviatoric stress invariant, P is the pressure including the overburden and e is the specific internal energy. The Y is the maximum stress difference or twice the maximum shear stress. The meaning of these parameters is indicated schematically in Figure 1.

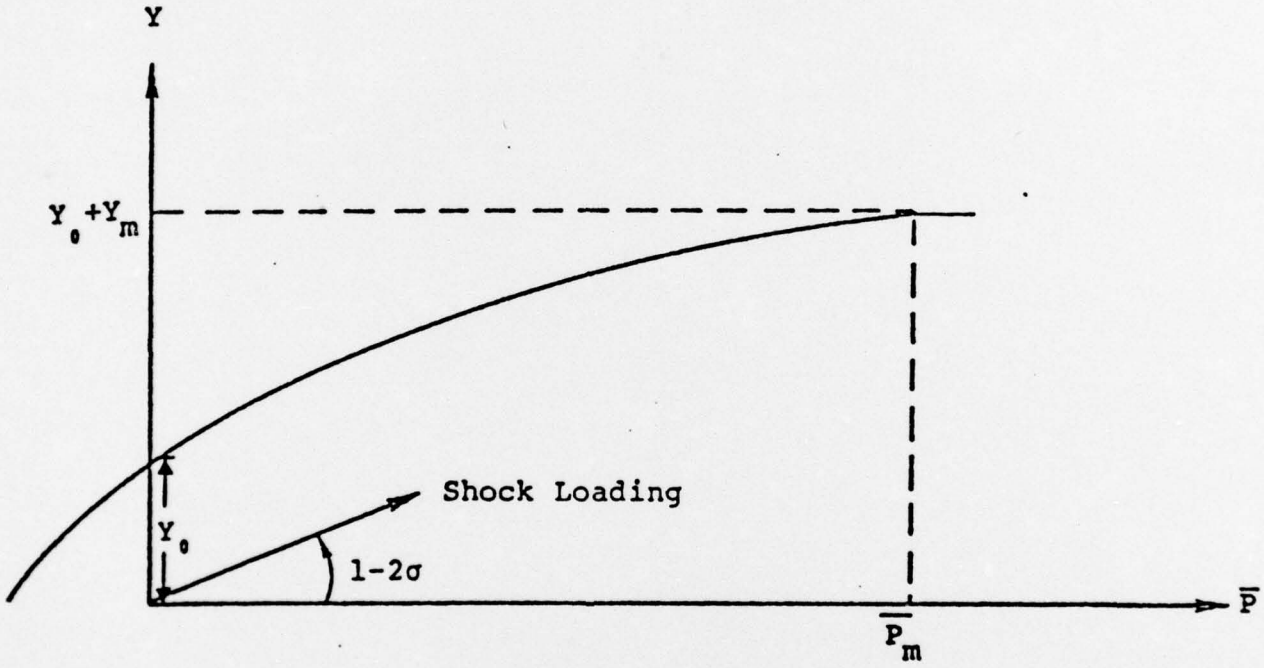

Figure 1. Assumed relationship between the material strength (Y) and the hydrodynamic component of stress ($\bar{P}$) for small e/e_m. When $\bar{P}$ is used for the abcissa the shock loading path has a slope of 1-2σ.

Table 1. Failure Envelopes for KASSERI Calculations

Calculation	Y_0 (kbar)	Y_m (kbar)	P_m (kbar)	e_m (10^{10} ergs/gm)
146	0.1	7.9	9.0	2.0
147	0.3	7.7	9.0	2.0
148	0.15	3.85	9.0	2.0
149	0.075	1.925	9.0	2.0

From the table we see that only the parameters Y_0 and Y_m were changed from calculation to calculation. The granite failure surface was used for 147. Calculations 148 and 149 are for the same failure surface with the strength cut by a factor of 2 and a factor of 4. Calculation 146 was done to see the effect of changing the shape of the failure surface while leaving the high pressure strength $(Y_0 + Y_m)$ unchanged.

The amplitude of the reduced velocity potential, $|\hat{\Psi}(\omega)|$, is plotted in Figure 2 for the four sources of Table 1. Also shown is the rhyolite source used for the MAST calculations reported by Barker, et al., (1976). The $\hat{\Psi}(\omega)$ is essentially the far-field displacement spectrum. In fact,

$$m_b \approx \log \alpha \hat{\Psi} (1 \text{ Hz}) ,$$
$$M_s \approx \log \mu \hat{\Psi} (0.05 \text{ Hz}) , \qquad (2)$$

as has been demonstrated theoretically in a number of past S^3 reports (e.g., Bache, et al., 1975a, 1975b).

In the following section we will be discussing the teleseismic body and surface waves that result from the source functions of Figure 2. However, we can draw some conclusions from the character of the source spectra alone.

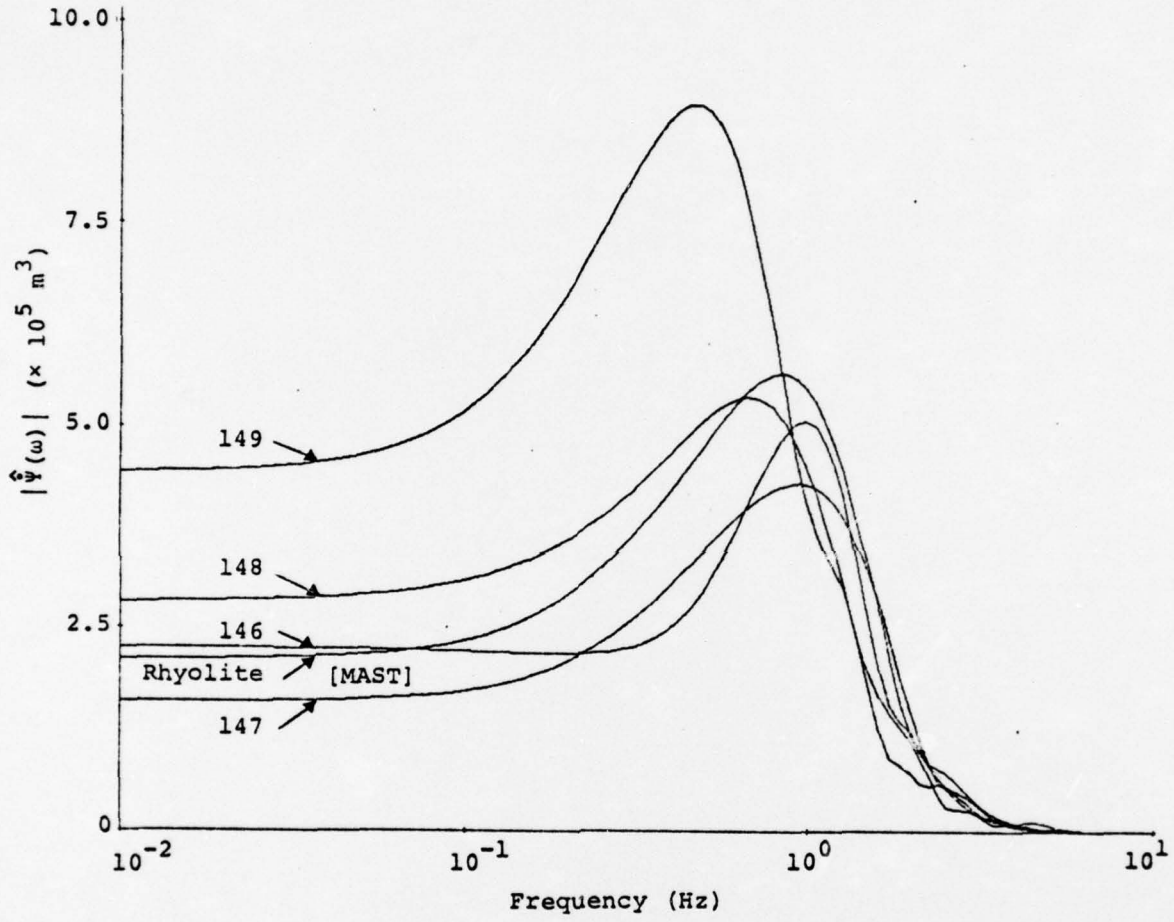

Figure 2. The source function amplitudes for the tuff sources of Table 1 and the rhyolite source used for MAST. The source functions are all scaled to 1000 KT.

In Table 2 are summarized the main characteristics of the spectra: The zero frequency limit (Ψ_∞), the peak value ($|\hat{\Psi}_p|$), the ratio of peak to zero frequency limit, the peak frequency (f_p) and the width of the peak at the amplitude halfway between Ψ_∞ and $|\hat{\Psi}_p|$. Comparing 146 and 147, we see that the low strength portion of the strength curve significantly narrows the peak while having a relatively minor effect elsewhere. Comparing 147, 148, 149, as the strength is decreased the spectrum gets larger. Also, the peak becomes narrower and moves to lower frequencies. The MAST source exhibits behavior between that of 147 and 148.

For MAST and KASSERI the important parameters controlling the teleseismic coupling are α = 4.2 km/sec, μ = 169 kbar for MAST and α = 3.1 km/sec and μ = 90 kbar for KASSERI. These values together with the source functions in Figure 2 and Table 2 give a first estimate of the relative size of the body and surface waves for these two events. Detailed comparison of theoretical and actual seismograms is made in the following section.

Table 2. Source Function Characteristics at 1000 KT

Source	Ψ_∞ ($\times 10^5 m^3$)	$\lvert\hat{\Psi}_p\rvert$ ($\times 10^5 m^3$)	$\lvert\hat{\Psi}_p\rvert/\Psi_\infty$	f_p (Hz)	Peak Width (Hz)
146	2.25	5.05	2.24	0.96	0.70
147	1.60	4.30	2.69	0.93	1.18
148	2.90	5.35	1.84	0.67	0.76
149	4.40	8.95	2.03	0.47	0.54
MAST	2.10	5.70	2.71	0.84	1.00

III. TELESEISMIC GROUND MOTION PREDICTIONS FOR KASSERI

In our report on MAST (Barker, et al., 1976) we outlined the procedure followed to predict the short and long period seismograms at selected SDCS stations. For KASSERI we follow the same procedure. Using the best available information for the rock properties at the working point, we compute an equivalent elastic source (RDP) for the explosion. This was discussed in the previous section. We also construct a layered earth model for the source vicinity from available information. The remainder of the calculation is identical for the two events.

In this section we discuss the theoretical body and surface waves for KASSERI and compare them to observations. For comparison we also include the MAST results.

3.1 EARTH MODELS FOR THEORETICAL BODY WAVE CALCULATIONS

The source region crustal structure for KASSERI is tabulated in Table 3. The top two kilometers of this structure are different from that for MAST; below that the two structures were taken to be the same.

Modeling of the remainder of the travel path is as described in our MAST report. For the structure at the receiver an average crustal model having little effect on the seismograms was used at all stations. This model, which is tabulated in Table 4, was chosen for the lack of any better information. For the upper mantle we chose a slightly modified version of the Helmberger and Wiggins (1971) model HWNE. The P wave-depth profile for this model, together with the revised version, HWNE-3, is shown in Figure 3.

The other factor to be selected is the parameter T/Q which characterizes the attenuation along the path. Results will be shown for two values of T/Q, 1.05 and 0.95.

Table 3. Source Region Crustal Structure for KASSERI

Depth (km)	Thickness (km)	α (km/sec)	β (km/sec)	ρ (g/cm³)
0.11	0.11	3.05	1.70	2.10
0.33	0.22	2.75	1.50	1.85
0.42	0.09	3.00	1.70	2.05
0.50	0.08	4.40	2.40	2.15
0.91	0.41	2.88	1.60	1.95
1.50	0.59	3.11	1.80	2.20
2.10	0.60	4.30	2.40	2.60
6.00	3.90	4.70	2.60	2.60
12.00	6.00	5.40	2.70	2.70
20.00	8.00	6.00	3.50	2.80

Table 4. Receiver Region Crustal Structure

Depth (km)	Thickness (km)	α (km/sec)	β (km/sec)	ρ (gm/cm³)
2.58	2.58	3.67	2.31	2.40
4.84	2.26	5.42	3.27	2.60
11.61	6.77	5.80	3.45	2.60
20.00	8.39	6.00	3.50	2.80

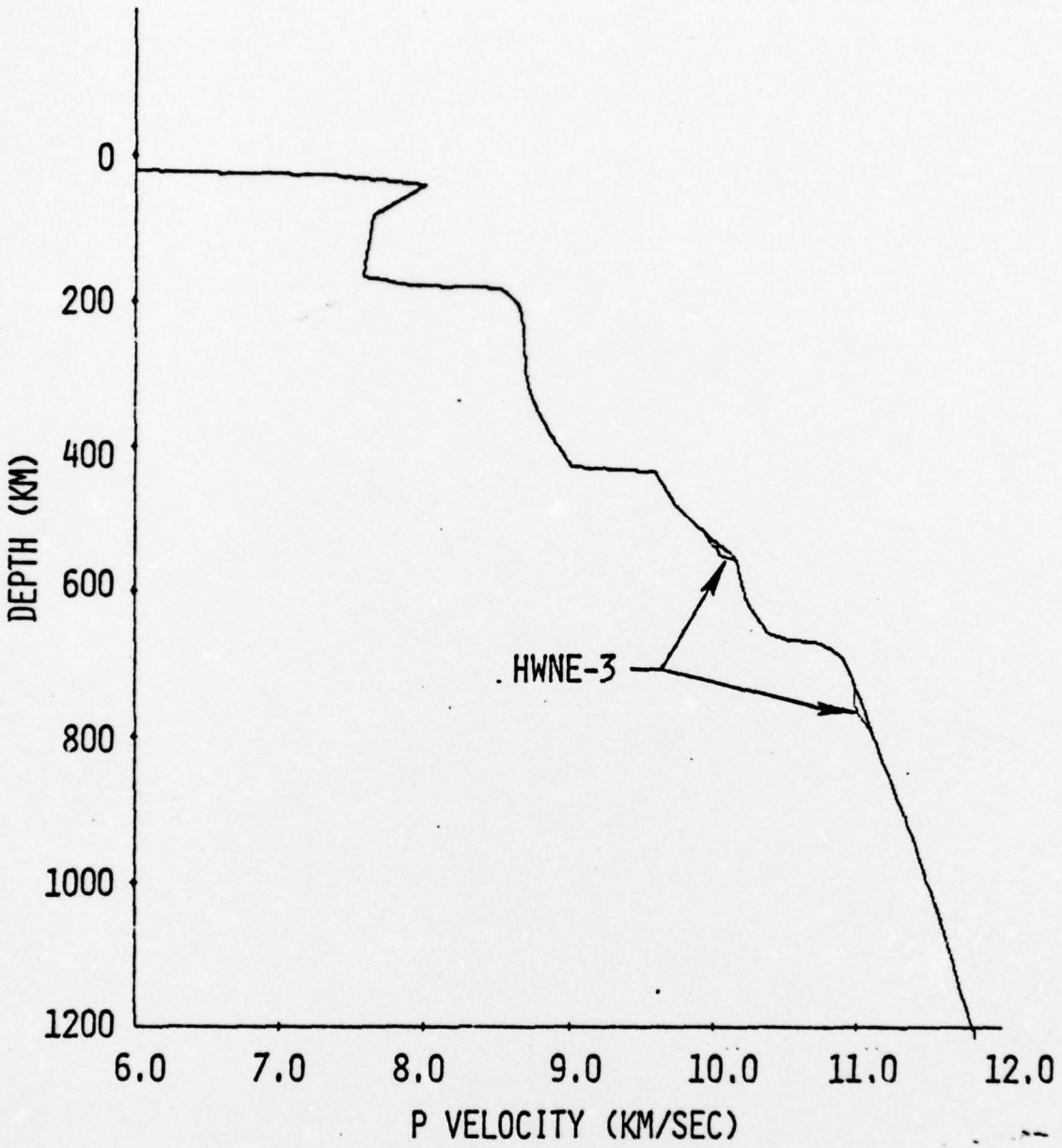

Figure 3. P velocity versus depth for the upper mantle model HWNE-3. This model is a slightly modified version of HWNE (Helmberger and Wiggins, 1971) with the differences as indicated in the figure.

3.2 COMPARISON OF THEORETICAL AND OBSERVED SHORT PERIOD RECORDINGS

We chose the source 148 (Figure 2) to be the most appropriate for the KASSERI event. In Section 3.3 we will compare seismograms for the four KASSERI sources with different failure envelopes, but for the comparison of theory and observations made here, 148 is the source. Note that this is the source with strength ($Y_0 + Y_m$) half that of granite.

The waveform comparisons are shown in Figure 4. For each of the five SDCS stations at which theoretical seismograms were made, we show first the comparison of theory and observations for MAST from Barker, et al., (1976), then the comparison for KASSERI. Comparing seismograms for the two events at each station, we can see how much the signals vary, both theoretically and as observed.

The differences between the two events are in the source material, as mentioned, and in the yield which is about twice as large for KASSERI as MAST. The distance to the stations of Figure 4 is approximately 10 km greater for KASSERI than MAST, a seemingly trivial change. Also, the near-source geology and burial depths change. The depths are H = 0.91 km for MAST and H = 1.26 km for KASSERI. The theoretical P - pP lag time is then approximately 0.50 seconds for MAST and 0.82 seconds for KASSERI.

Examining the observations, we see an extraordinary change in the shape of the RKON recording between the two events. At the other stations the differences are much less pronounced. In fact, at the other stations one could argue that the waveform differences are primarily the result of the change in P - pP lag time.

The theoretical seismograms were computed with T/Q = 0.95. We also computed the same stations with T/Q = 1.05

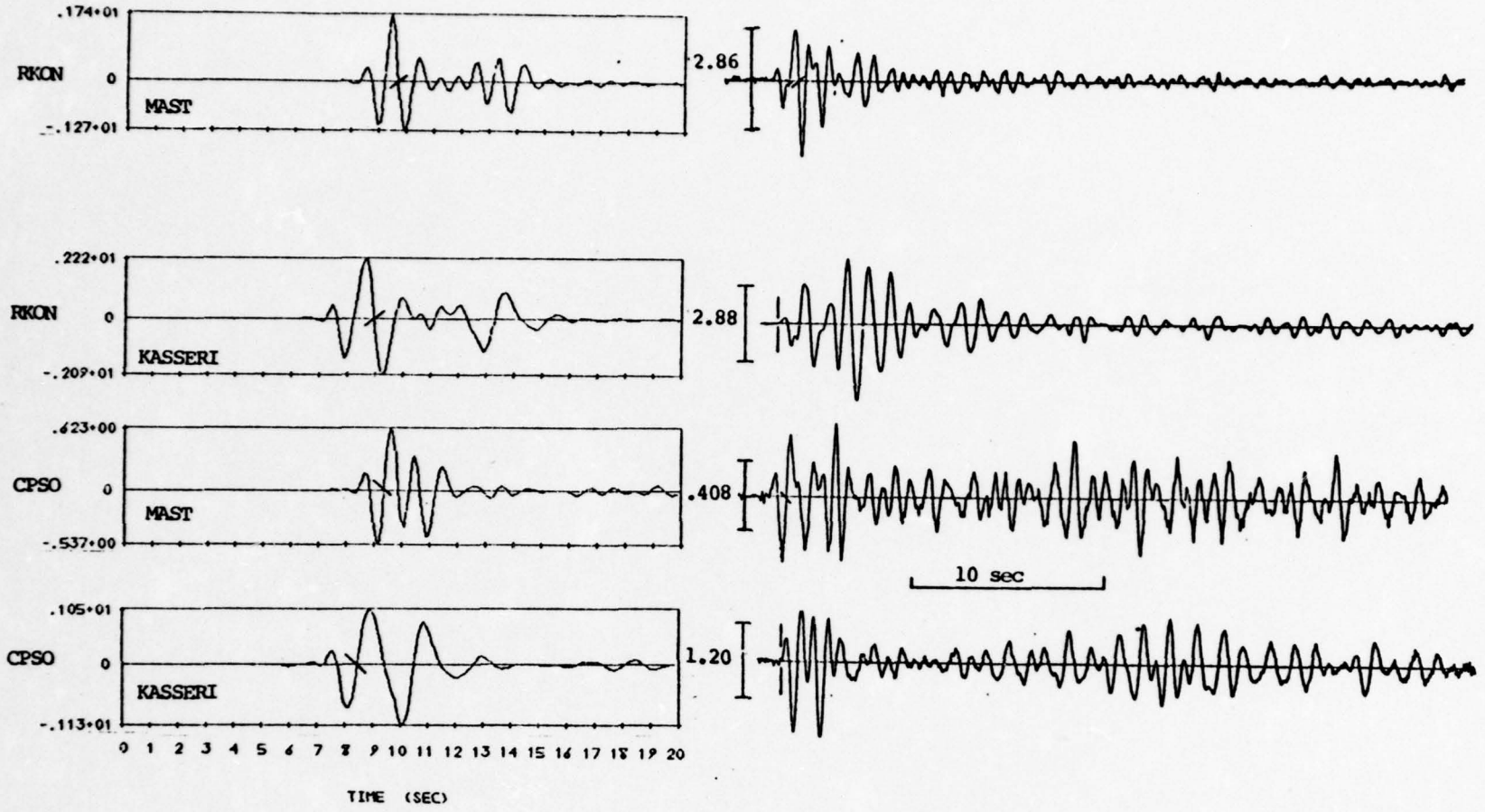

Figure 4. Comparison of synthetic (left) and observed short period vertical component seismograms at five SDCS stations for the events MAST and KASSERI. The amplitude at 1 Hz is indicated at the left on each record. The bars show the cycle at which the maximum or "d" amplitude measurements were made.

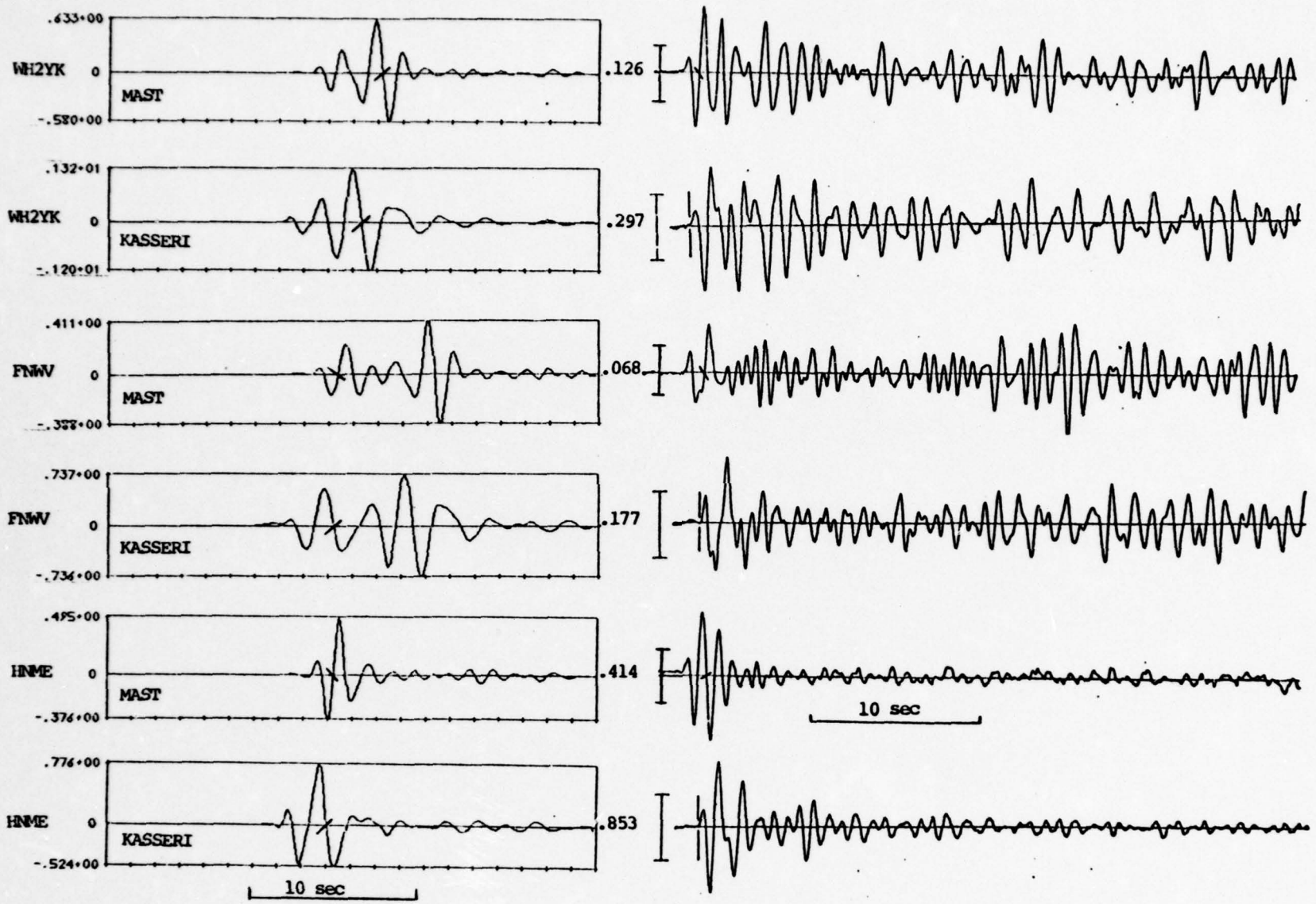

Figure 4. (Continued)

and will be discussing measurements made from both sets. For a visual comparison as in Figure 4, the difference between the two is hardly apparent. At each station the instrument response was taken from calibration data provided by the Project Officer. The calibration was done just prior to MAST but was used for KASSERI as well.

Regarding the comparison of theoretical and observed waveforms, we can only make the same comments as in the MAST report. The interference phenomena that seem to control the shape of the waveform at the nearer four stations are not adequately represented in our models. Our theoretical signals also fail to include much of the high frequency energy that appears after the first few seconds of the record.

The important fact is that it does appear that we have properly included the factors controlling the amplitude of the b phase, the first cycle on the record. This phase is least affected by phenomena not related to the explosion coupling into elastic waves – the feature presumably most indicative of explosion yield. Evaluation of the comparison should rely most heavily on the b phase data.

The comparison between theoretical and observed amplitudes from the seismograms of Figure 4 is shown in Figures 5 and 6. The data in Figure 5 are for the "b" phase; those in Figure 6 are for the maximum amplitude in the first three cycles, the "d" phase. Along with the plotted b and d amplitudes, the periods of the cycles at which these were measured appear on the figures.

With regard to the data of Figures 5 and 6 there are two important observations to be made. First, the amplitude and period of the "apparent ground motion" is dependent on the characteristics of the recording instrument. Unfortunately, it is not necessarily true that a plot of actual versus theoretical "true ground motion" amplitudes would

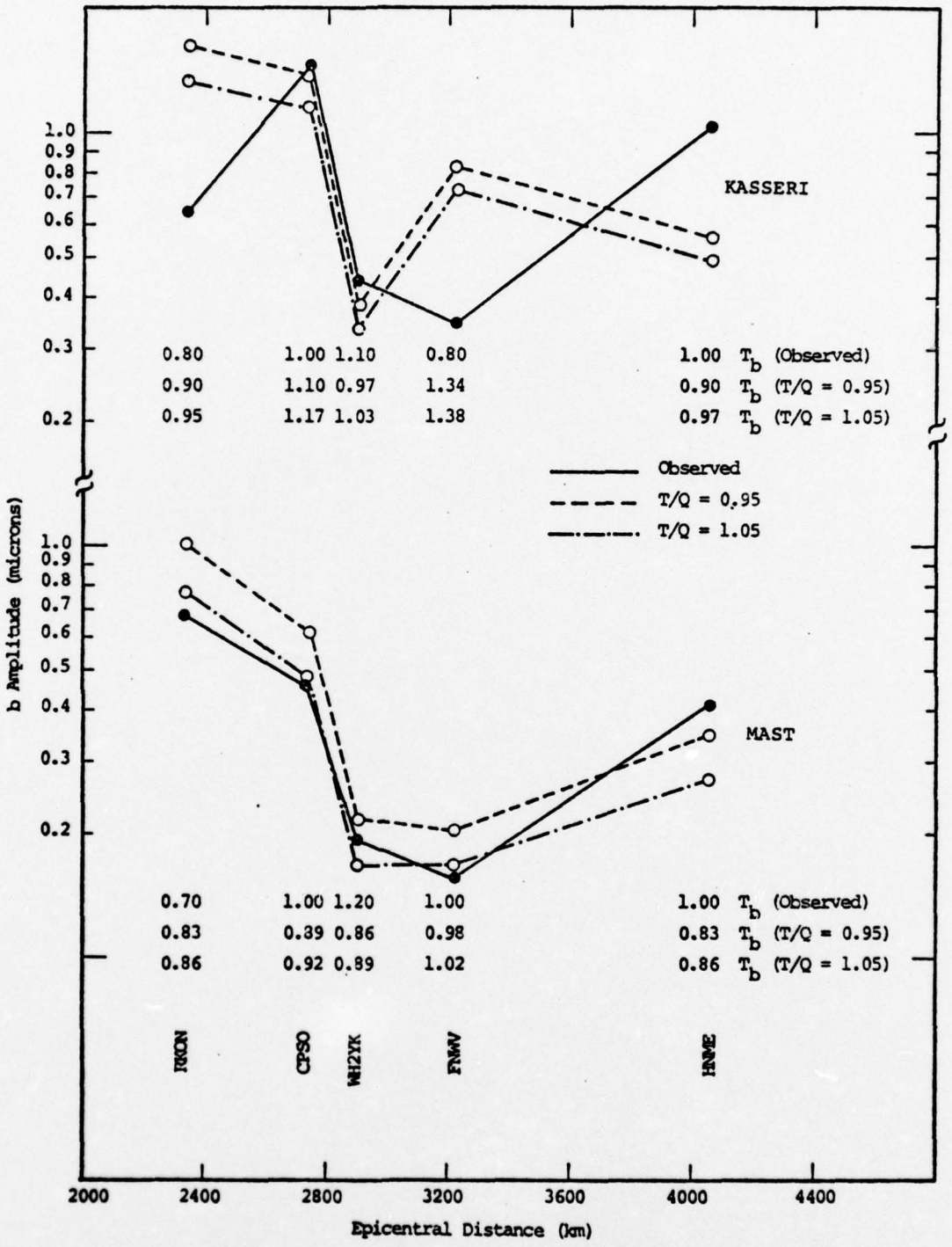

Figure 5. Comparison of theoretical and observed b amplitudes for MAST and KASSERI at five SDCS stations. Seismograms were computed for two values of T/Q as indicated. The KASSERI source function is denoted 148 and the upper mantle model is HWNE-3.

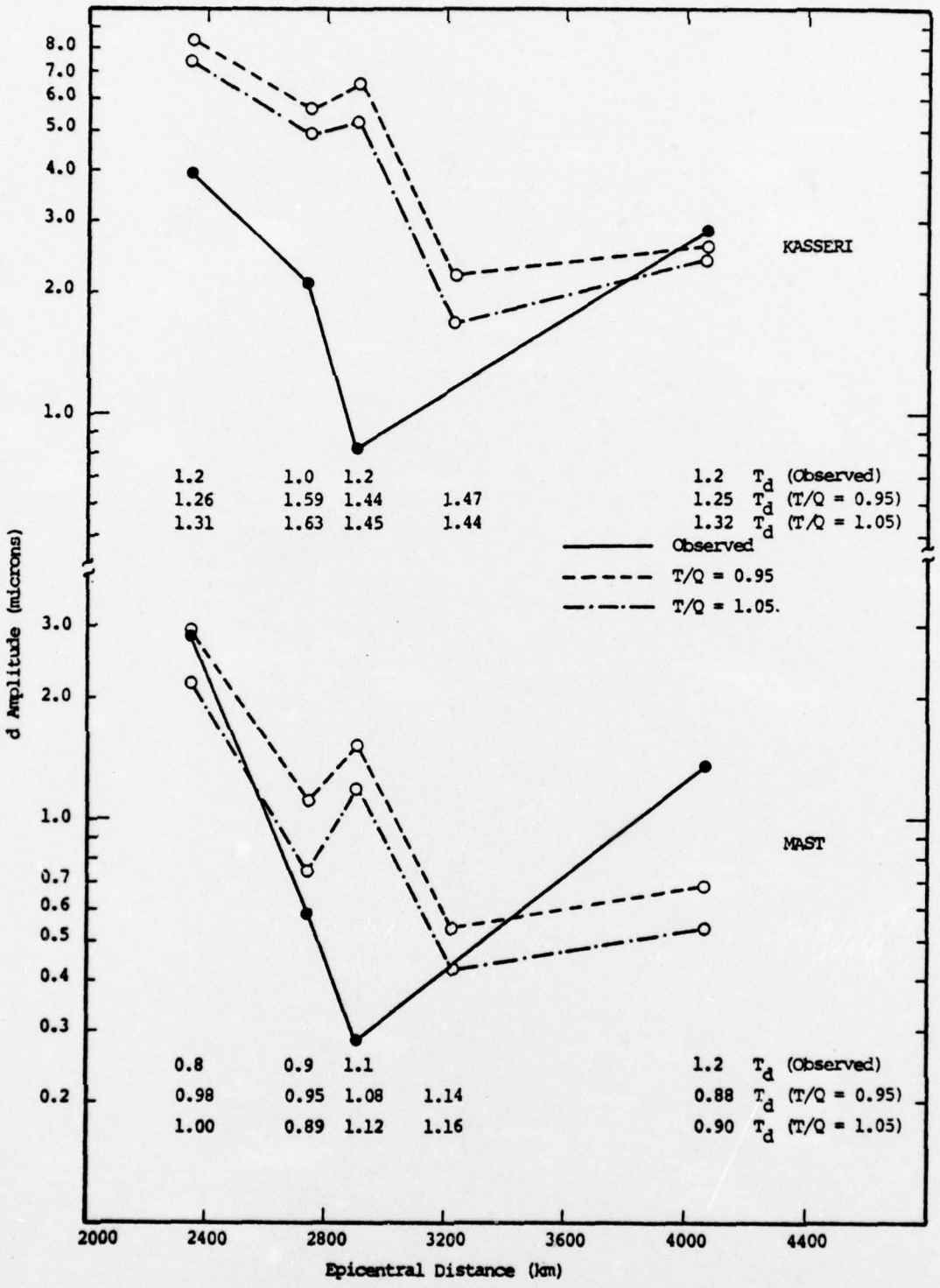

Figure 6. Comparison of theoretical and observed d amplitudes for MAST and KASSERI.

have the same appearance as the plots of Figures 5 and 6. This is because the instrument correction to true ground motion, as conventionally used, has an erratic effect. This subject is discussed in some detail in Appendix A where we show the results of the following numerical experiment: (1) The theoretically computed ground motion for the KASSERI event at HNME is filtered by six different short period instruments; one being specified by LRSM nominal instrument response curves and the others specified by calibration data provided by the Project Officer for the five SDCS stations. (2) Synthetic seismograms were computed. (3) Amplitudes were measured in the conventional way; since the entire process is done digitally, the errors in the measurement of amplitude and apparent period can be reduced to nearly vanishing.

The result of the numerical experiment outlined above is somewhat surprising. The apparent period is used to determine an instrument correction to what we shall call "apparent ground motion". Even though the actual ground motion is identical, the apparent ground motion varies over a large range; as much as a factor of two! It turns out that the discrepancy would be much reduced if no instrument correction were applied.

The second point is closely related to the first made above. We find that we must know the instrument response quite accurately to be able to compute theoretical seismograms that are comparable to the actual observations. But how well do we know this response? How carefully are the instruments calibrated? At present we have no way of making a judgement.

The "observed" data plotted in Figures 5 and 6 are based on amplitude and period measurements made at S^3. Once again, the instrument correction problem arises. We believe that the amplitudes appearing in the SDCS Event Reports

(No. 18 for MAST and No. 41 for KASSERI) were corrected for instrument response using LRSM nominal curves. We used the specific instrument curves provided by the Project Officer. These were based on calibrations carried out just before MAST and we can only hope that they remained valid for KASSERI – both for the observations and for synthesizing seismograms.

From the comparison of Figures 5 - 6 we draw the following conclusions:

- The scaling of observed amplitudes between the two events is quite consistent except for RKON. We previously pointed out the marked dissimilarity in waveforms at RKON for these two events.
- The match between theoretical and observed amplitudes is about the same for the two events. The exceptional stations are RKON and FNWV. It will be very difficult to explain the RKON anomaly with present techniques since the epicentral distance variation between events is only 0.1 degrees. Waveform similarities at WH2YK, CPSO and HNME discourage attempts to attribute the anomaly to near-source effects. Even in our theoretical model the interference pattern at FNWV is enough to make the b amplitude behave erratically as we see by comparing results for the two events. However, it is unlikely that current modeling techniques, no matter how accurately used, would permit a very accurate duplication of observed records at this station.
- The scaling between the two computed source functions seems to be approximately correct. Perhaps the MAST source is slightly large compared to KASSERI.

- Differences between theoretical and observed amplitudes are less than a factor of two nearly everywhere. A goodly portion of the discrepancy can likely be attributed to inaccuracy in the upper mantle model. More extensive studies employing much more data could improve this model and therefore the agreement at individual stations.
- Changing T/Q from 0.95 to 1.05 increases the period of the phase measured by ≈ 0.03 - 0.07 seconds. The increase in amplitude is 15 - 25 percent.
- The periods of the b phase generally agree with the observations. If anything, they may be a little too short on the average. For the d phase the theoretical periods tend to be a bit too long.
- Clearly, the further we go into the record, the poorer the match between theory and observations. However, the further one goes into the record, the greater the effect of factors other than the coupling of explosion energy into elastic waves. Hence the emphasis on the b phase.

3.3 THE EFFECT OF MATERIAL STRENGTH ON TELESEISMIC BODY WAVE RECORDINGS

The KASSERI calculations of the previous section were done with the source 148. How much different would the results be if we had used one of the other three sources of Table 1? We compare the four sources, which vary only in the specification of the material strength, by computing seismograms for station HNME with T/Q = 1.05. The seismograms are shown in Figure 7. The b amplitudes were measured from these records and are plotted versus the limiting material strength ($Y_0 + Y_m$) in Figure 8. Also shown is the period of the b measurement. Since these seismograms were computed with the LRSM nominal instrument response, direct comparison with the KASSERI observations is not possible. However, in Appendix A,

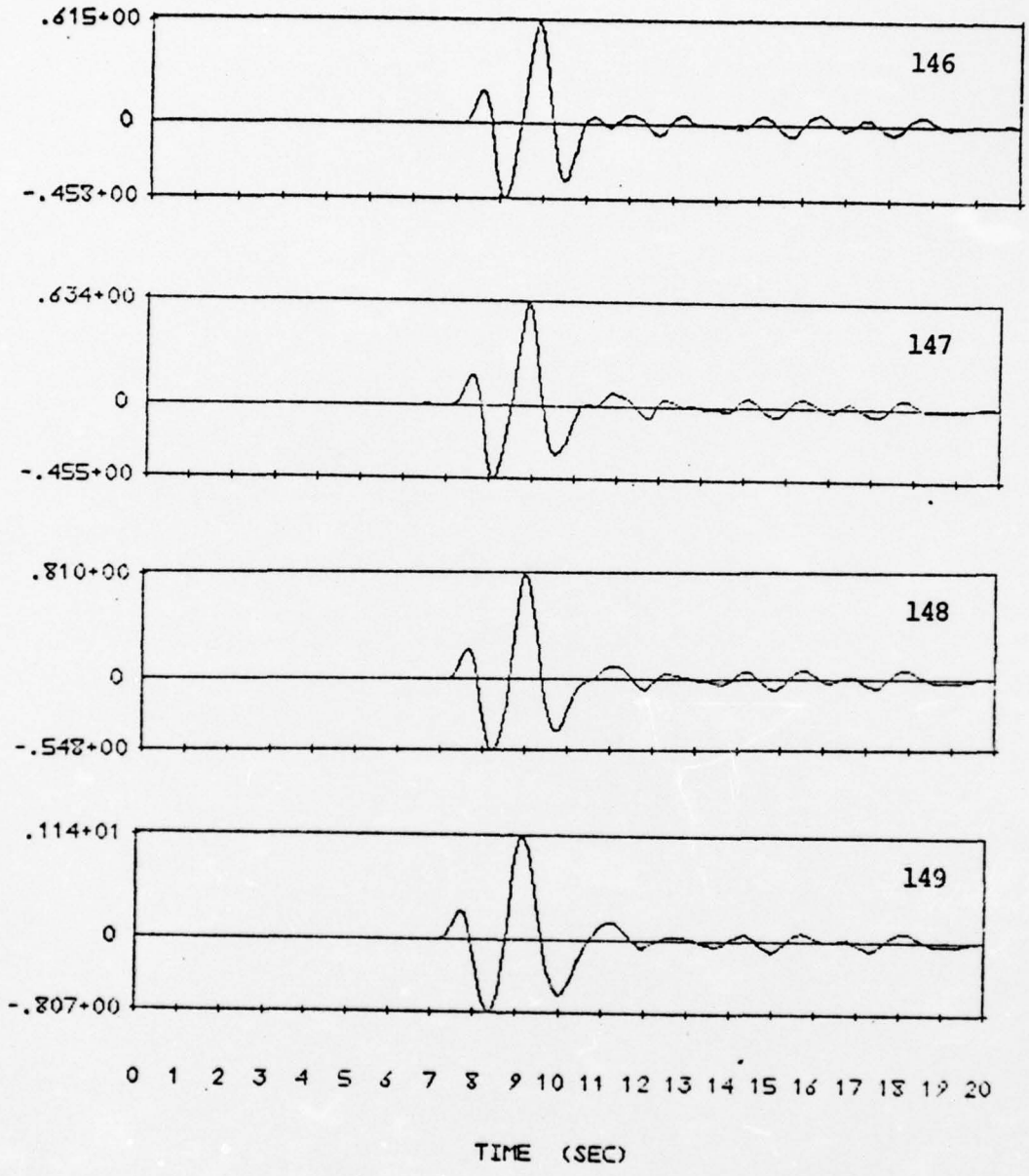

Figure 7. Synthetic seismograms at HMNE for the four tuff source functions of Table 1. The parameters of the calculation are the same as for Figure 4 except T/Q = 1.05 and the LRSM instrument response was used.

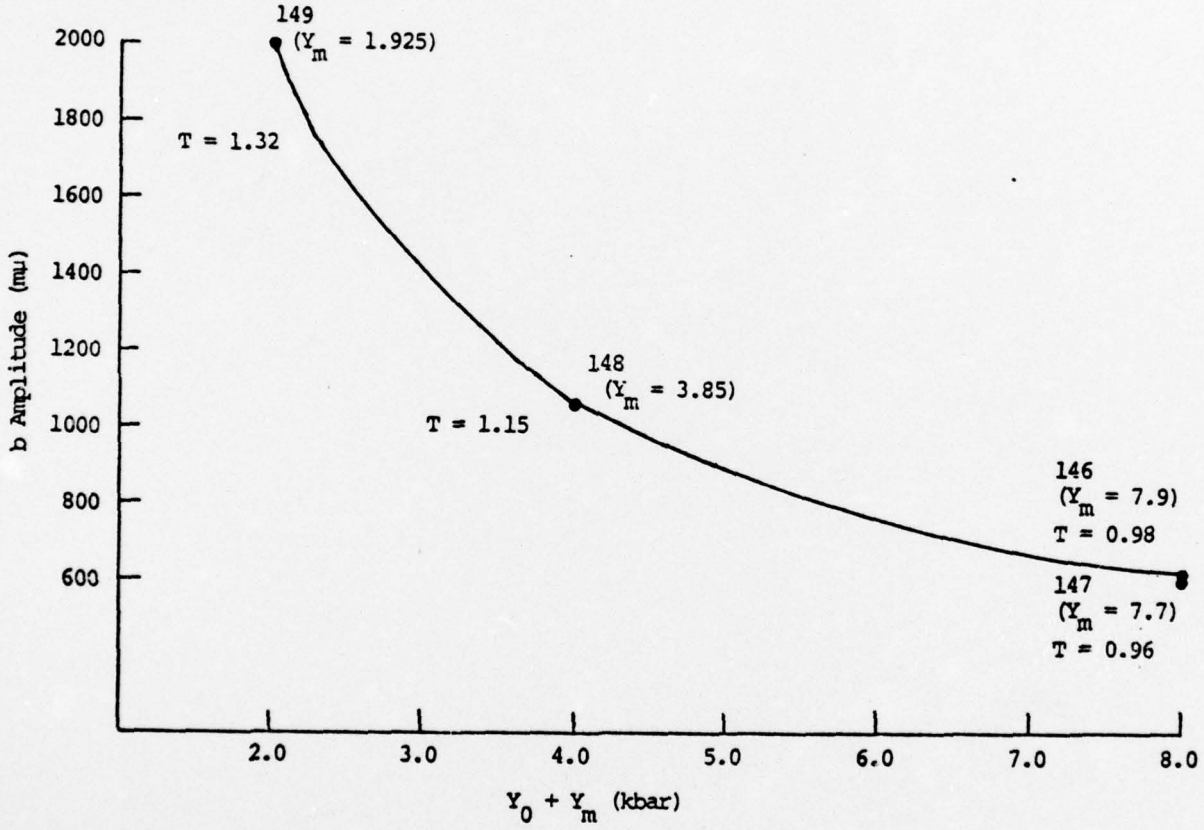

Figure 8. The b phase measurements for theoretical seismograms at HNME computed with four source functions. The source functions represent KASSERI tuff with four different estimates of material strength. The instrument response was the LRSM nominal.

Table A.2, we show that the HNME specific instrument gives a b phase amplitude that is 0.46 as large and a period that is 0.19 seconds shorter than that for the LRSM applied to the ground motion from source 148.

The b phase data of Figure 8 is consistent with our discussion of the spectral characteristics of the four source functions (Figure 2) given in Section II. The amplitude increases with decreasing strength and the rate of increase is more rapid at lower strength. The period of the waveform increases rapidly with decreasing strength due to the shift in corner frequency. For b amplitude there is essentially no difference between the two sources (146 and 147) that have the same ultimate strength as granite, even though the shape of the yield surface is different.

Which of the sources is most appropriate for KASSERI? In the previous section we saw that 148 was reasonably successful. If in error, one would think 148 to be too low in amplitude and to have too little energy (relatively) in the high frequencies. We see in Figure 7 that improvements in these two features require adjustment in the strength in opposite directions. Also, a strength of about half that of granite seems reasonable. If we are satisfied with the MAST source, a KASSERI source which scales to the MAST source in a manner consistent with the observations is also required. Source 148 seems to fulfill this criterion fairly well. For all these reasons, we selected the source 148 as being most representative of KASSERI. The data of Figure 8 are quite important as an indication of the effect of erroneous estimates of material strength.

3.4 COMPARISON OF THEORETICAL AND OBSERVED RAYLEIGH WAVES FOR KASSERI

In the MAST report (Barker, et al., 1976) we selected an appropriate average crustal model for the travel path between NTS and the five SDCS stations. Basically, we began

with published models that seemed appropriate, then perturbed them slightly to bring the theoretical group velocity dispersion curves and travel times into close agreement with the observed. The observed curves were computed directly from the MAST observations using the S^3 data analysis program MARS (Savino, et al., 1975). The dispersion curves for the revised models fit the observations to within 0.04 km/sec for periods between 10 and 30 seconds. The models were CIT109-A for WH2YK, MCEV-J for RKON and MCEV-B for CPSO and FNWV. Velocity-depth profiles for these models appear in the MAST report. The published models on which they are based are CIT109 (Archambeau, et al., 1969) and MCEV (McEvilly, 1964). Only the model MCEV-J differs to any substantial degree from the starting model. For the attenuation we used the model of Tryggvason (1965).

For the theoretical Rayleigh waves for KASSERI, we use the same earth models as for MAST. We had previously verified the fact that the group velocity dispersion is essentially unchanged from one NTS event to another. For the station HNME for which there were no MAST observations, we developed a new model, MCEV-ϕ, which matches the group velocity dispersion.

Comparison of the theoretical and observed Rayleigh waves at the five SDCS stations are shown for both MAST and KASSERI in Figure 9. The radial and vertical components are both shown.

Regarding the observations, we first comment on the remarkable similarity in the recorded waveforms for the two events. The fact that they are so similar allows us to point out with some confidence that the radial component for KASSERI at RKON has polarity reversed. Also, the time marks given in the SDCS Event Reports for these two events are certainly incorrect in many instances. We have indicated (T) the reported travel time for the Airy phase on each seismogram. The inconsistencies in T between MAST and

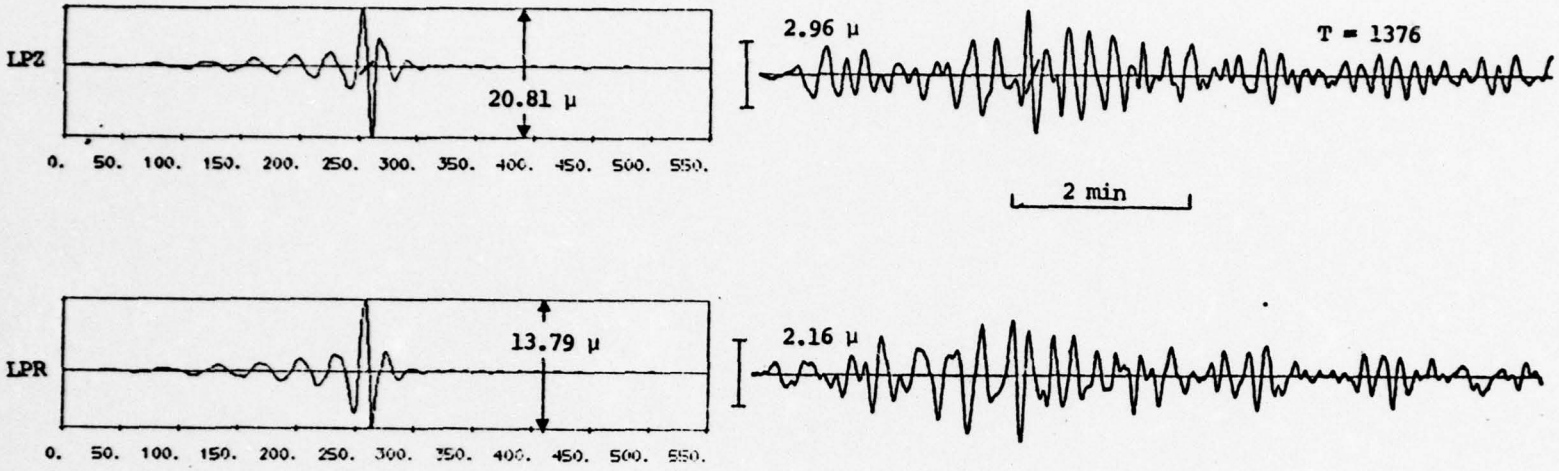

Figure 9. Comparison of theoretical and observed Rayleigh waves at five SDCS stations. Both the vertical and radial components are shown for MAST and KASSERI. The amplitude at 25 seconds is indicated on each record. The bar on the vertical records indicates the cycle at which the Airy phase amplitude was measured. The travel time for this phase is indicated on the observations by T. These values, taken from the SDCS event reports, appear to be incorrect in many cases.

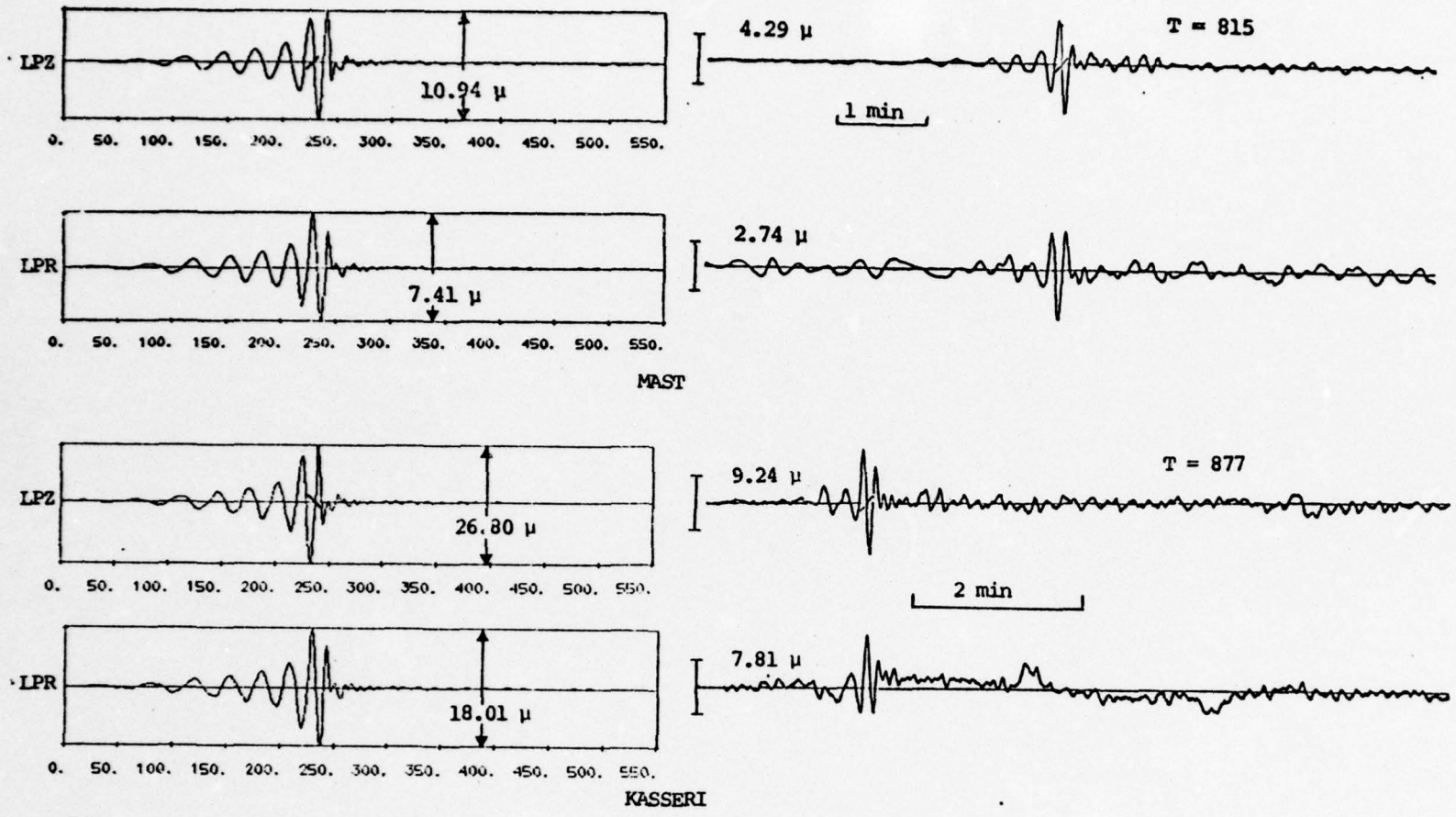

Figure 9. (Continued)

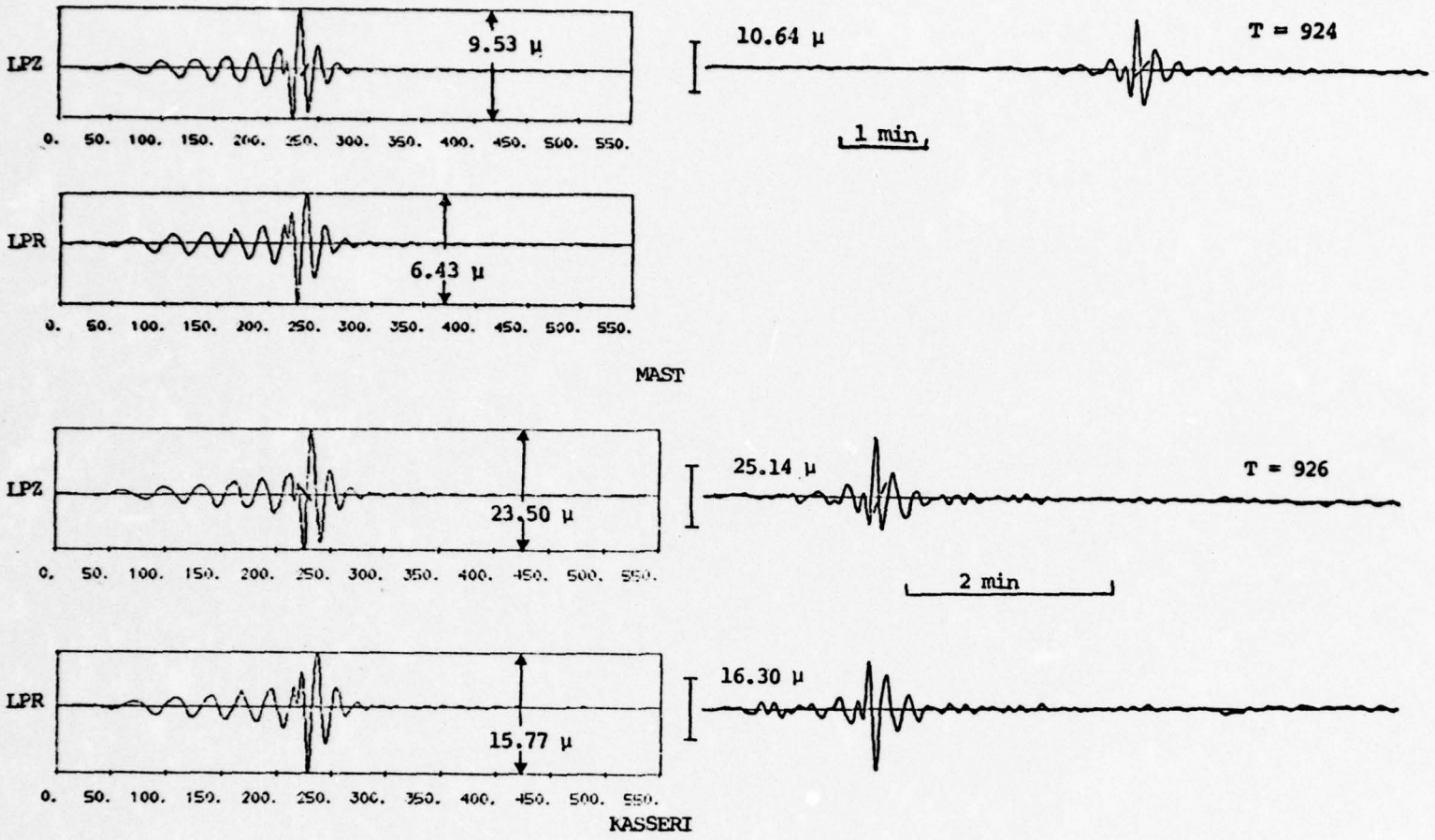

Station CPSO

Figure 9. (Continued)

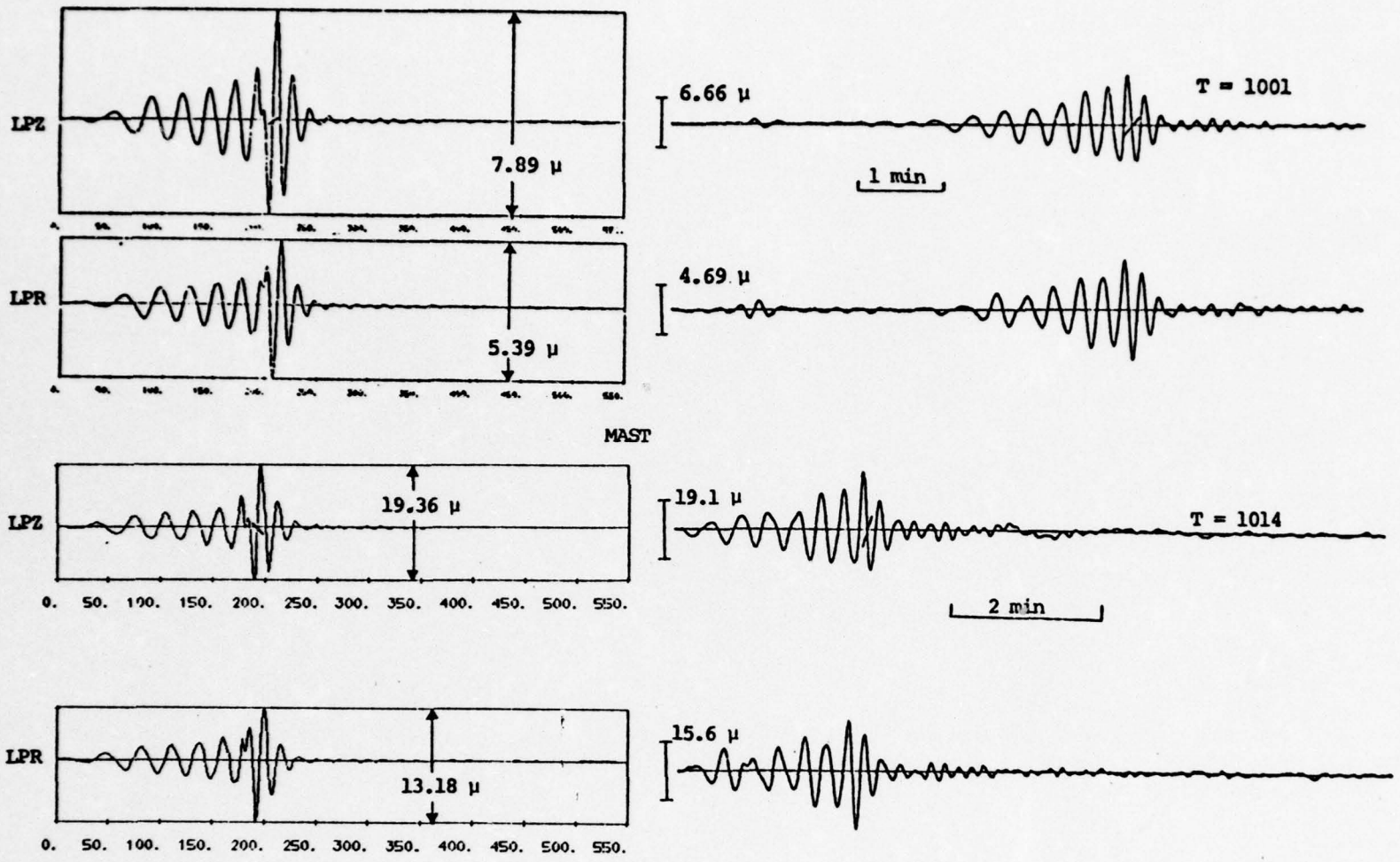

Station WH2YK

Figure 9. (Continued)

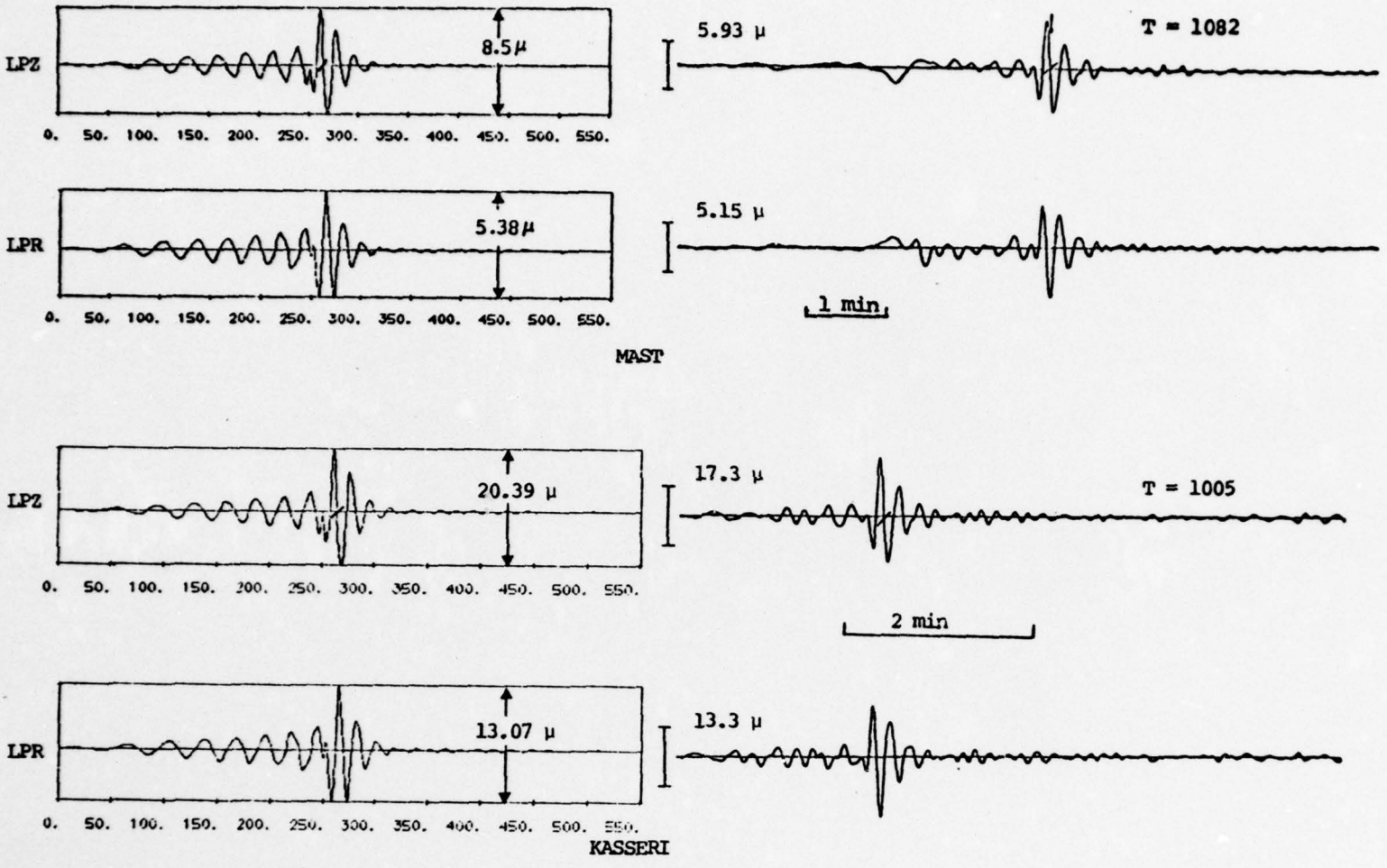

Figure 9. (Concluded)

KASSERI and the deviation from previous experience at these stations are considerable.

In computing the KASSERI synthetic seismograms the only thing different from MAST is the source and the source depth. As we see in the synthetics of Figure 9, this difference has little effect on the waveform. The agreement between synthetic and observed waveforms is then the same for the two events and seems to be reasonably good considering the simple procedure followed to select an earth model.

One question that must arise in discussing the seismograms of Figure 9 is the instrument response. We discussed the instrument effect on body wave amplitudes at some length in previous sections. As mentioned, we were given instrument calibration data for the seismometers at each of the five SDCS stations. The calibration data indicated that the LPZ instrument response differed from the LRSM nominal response by a not insignificant degree. We first computed synthetics using the LRSM nominal response curves. When we then computed with the calibration response, we found the match between synthetic and observed seismograms to deteriorate considerably. In fact, in some cases no satisfactory seismogram could be computed at all. We conclude that the calibration data is incorrect or not sufficiently complete. All of our results are then based on seismograms computed with the LRSM nominal responses and these appear in Figure 9. The effect of this inconsistency is unknown.

We still must make amplitude measurements from the observations and an instrument correction must be applied. For the surface wave amplitudes given in the MAST and KASSERI shot reports, we believe the instrument correction was based on the LRSM nominal LP response curves. But are these appropriate? We decided that the amplitude response portion of the calibration data is probably correct and our problems are due to the phase data. Therefore, we recomputed

the Airy phase amplitude using the amplitude calibration data for the specific station.

The comparison between theoretical and observed Airy phase amplitude for the vertical component of the Rayleigh wave is shown in Figure 10. Also shown on the figure are the amplitudes given in the SDCS shot reports. We see that at the Airy phase period there can be a rather large difference between the LRSM nominal instrument response and that from the individual instrument calibration.

The agreement between theoretical and observed amplitudes is essentially the same for the two events. Certainly the agreement at individual stations can be improved and we will say more about that below. First, we want to point out that, as with the body waves, the scaling between the MAST and KASSERI source functions seems to be nearly correct. This is important because the body and surface waves sample different portions of the source spectrum and are proportional to different source material properties as was pointed out in (2). In our theoretical formulation the vertical component of surface wave spectrum is computed from (Harkrider, 1964),

$$\bar{\omega}_0 = 4\pi \mu \hat{\Psi}(\omega) \frac{K_S}{c_R} \underset{\sim}{A}_R H_0^{(2)}(k_r r) , \qquad (3)$$

where $\underset{\sim}{A}_R$ is the amplitude response of the layered medium, c_R is the Rayleigh wave speed and $k_r = \omega/c_R$. These quantities all depend only on the properties of the average path crustal model. Then, observing that $\hat{\Psi}(\omega) \to \Psi_\infty$ at the low frequencies of interest, we see that for two explosions with a common travel path,

$$\frac{\bar{\omega}_0^{(1)}}{\bar{\omega}_0^{(2)}} = \frac{\mu^{(1)} \Psi_\infty^{(1)} K_S^{(1)}}{\mu^{(2)} \Psi_\infty^{(2)} K_S^{(2)}} , \qquad (4)$$

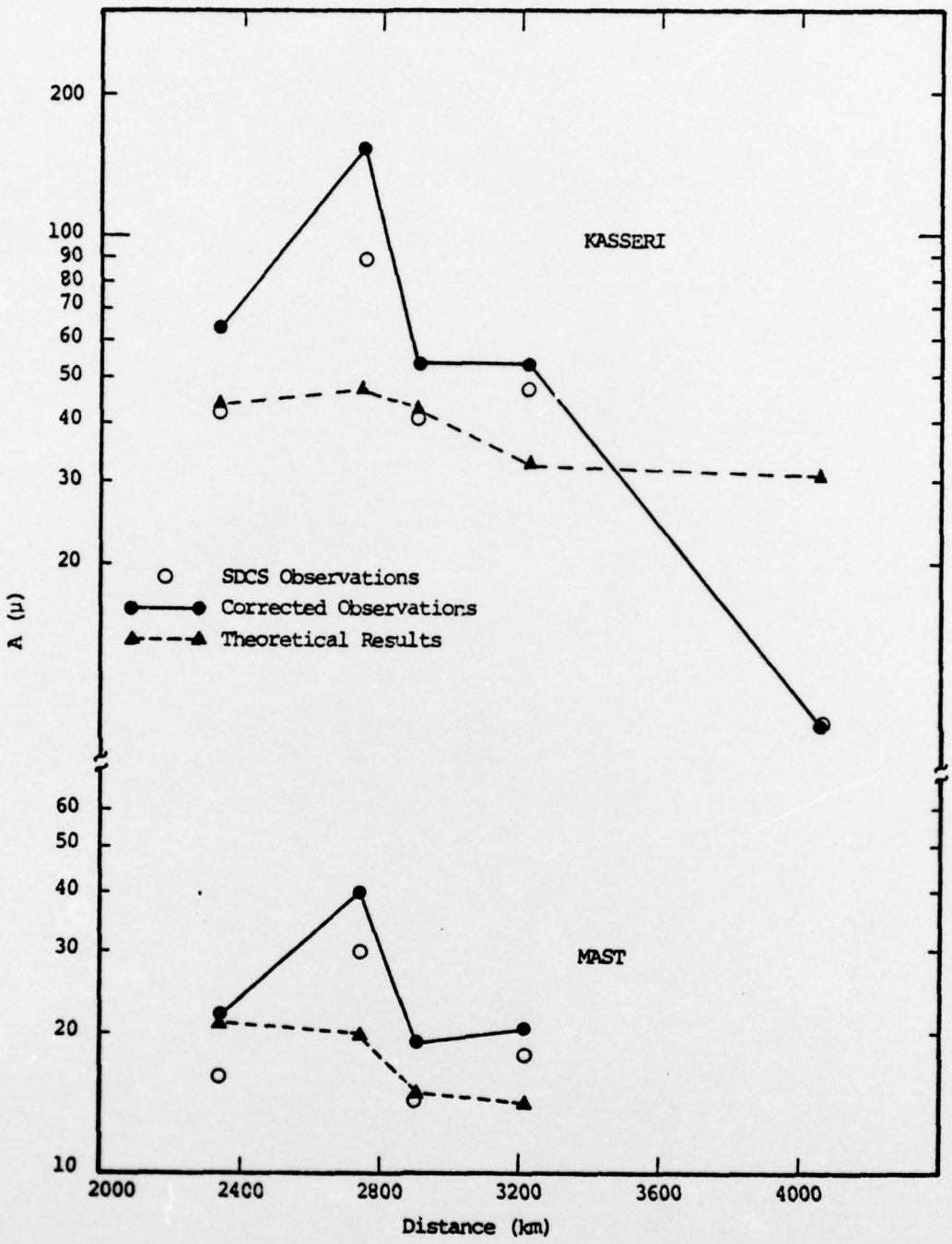

Figure 10. Comparison of theoretical and observed Airy phase amplitudes at five SDCS stations for KASSERI and MAST. Two observed values are shown; one set (SDCS) apparently used the LRSM nominal response curves and we corrected for the calibration response data.

where K_S is a depth dependent Rayleigh wave excitation factor. For MAST and KASSERI the μ values are 169 kbar and 90 kbar, respectively. The Ψ_∞ for the two events are given in Table 2, scaled to 1000 KT. The K_S is frequency dependent, but in the Airy phase period range of 13 - 17 seconds, the K_S for MAST is about 0.81 times that for KASSERI. Using 148 for KASSERI, this theoretical scaling of surface waves seems to be the same as the scaling of the observations as we see in Figure 10.

The procedure used to select an average crustal model for the travel path is fairly crude and better models could certainly be obtained. The discrepancy in the observed and theoretical relative amplitudes from station to station in Figure 10 must be in large part due to deficiencies in the travel path models. This assertion is born out by comparison of the MAST and KASSERI observations with data from previous NTS explosions. Von Seggern (1973) analyzed some 686 Rayleigh wave amplitudes from North American LRSM recordings of 43 NTS explosions. Using a procedure he calls Joint Magnitude Determination, he fit these data to the unified distance relation:

$$\log A_{ij} = 4.25 - 0.90 \log r_{ij} + \hat{F}_j + \hat{C}_i \ , \qquad (5)$$

where A is amplitude, r is epicentral distance, $\hat{F}_j$ is an event correction and $\hat{C}_i$ is a station correction. Using Von Seggern's $\hat{C}_i$ we can determine how the SDCS sites have coupled on the average. These data, normalized to RKON amplitudes, are summarized in Table 5. We notice that the relatively high amplitude at CPSO is consistent with past experience. Von Seggern's data suggest that WH2YK should also give a relatively large amplitude, but we do not see that with MAST or KASSERI. For FNWV no $\hat{C}_i$ is available and the KASSERI HNME observation seems to be low compared with past experience.

Table 5. Relative Rayleigh Wave Amplitudes for MAST and KASSERI Compared to Average Values Given by Von Seggern (1973)

Station	C_i	Average Relative Amplitude	MAST Relative Amplitude	KASSERI Relative Amplitude
RKON	-0.20	1.0	1.0	1.0
CPSO	0.17	2.0	2.7	2.4
WH2YK	0.12	1.7	0.7	0.83
FNWV	--	--	1.2	0.83
HNME	-0.20	0.60	--	0.14

IV. REFERENCES

Archambeau, C. B., E. A. Flinn, and D. G. Lambert (1969), "Fine Structure of the Upper Mantle," J. Geophys. Res., 74, 5825-5865.

Bache, T. C., J. T. Cherry, K. G. Hamilton, J. F. Masso, and J. M. Savino (1975a), "Application of Advanced Methods for Identification and Detection of Nuclear Explosions from the Asian Continent," Systems, Science and Software Report SSS-R-75-2646, May.

Bache, T. C., J. T. Cherry, N. Rimer, J. M. Savino, T. R. Blake, T. G. Barker, and D. G. Lambert (1975b), "An Explanation of the Relative Amplitudes of the Teleseismic Body Waves Generated by Explosions in Different Test Areas at NTS," Systems, Science and Software Final Report for DNA, October.

Barker, T. G., T. C. Bache, J. T. Cherry, N. Rimer, and J. M. Savino (1976), "Prediction and Matching of Teleseismic Ground Motion (Body and Surface Waves) from the NTS MAST Explosion," Systems, Science and Software Report SSS-R-76-2727 (Draft).

Cherry, J. T., N. Rimer, and W. O. Wray (1975), "Seismic Coupling from a Nuclear Explosion: The Dependence of the Reduced Displacement Potential on the Nonlinear Behavior of the Near Source Rock Environment," Systems, Science and Software Report SSS-R-76-2742, September.

Harkrider, D. G. (1964), "Surface Waves in Multilayered Media. I. Rayleigh and Love Waves from Sources in a Multilayered Half-Space," Bull. Seism. Soc. Amer., 54, 627-679.

Helmberger, D. V., and R. A. Wiggins (1971), "Upper Mantle Structure of the Midwestern United States," J. Geophys. Res., 76, 3229-3245.

McEvilly, T. V. (1964), "Central U. S. Crust - Upper Mantle Structure from Love and Rayleigh Wave Velocity Inversion," Bull. Seism. Soc. Am., 54(6).

Riney, T. D., J. K. Dienes, G. A. Frazier, S. K. Garg, J. W. Kirsch, D. H. Brownell, Jr., and A. J. Good (1972), "Ground Motion Models and Computer Techniques," DNA-2915Z, Systems, Science and Software Report 3SR-1071.

Savino, J. M., T. C. Bache, J. T. Cherry, K. G. Hamilton, D. G. Lambert, and J. F. Masso (1975), "Application of Advanced Methods for Identification and Detection of Nuclear Explosions from the Asian Continent," Systems, Science and Software Report SSS-R-76-2792, December.

Tryggvason, E. (1965), "Dissipation of Rayleigh Wave Energy," J. Geophys. Res., 70(6),

von Seggern, D. (1973), "Joint Magnitude Determination and Analysis of Variance for Explosion Magnitude Estimates," Bull. Seism. Soc. Am., 63(3).

APPENDIX A
EFFECT OF INSTRUMENT RESPONSE ON MEASURED AMPLITUDES

Standard procedure for determining ground motion amplitudes from seismograph recordings requires correction for the instrument response at the apparent period of the cycle being measured. There are several possible sources of error in this procedure:

1. The signal is not monochromatic and a single period correction factor can never entirely remove the instrument effect.
2. The amplitude and phase response of the instrument at the time the signal is recorded may not be accurately known.
3. It is often difficult to accurately measure the dominant period of the cycle being measured.

These are all sources of error that refer to a single recording by a single instrument. While everyone knows they exist, a quantitative estimate of their effect is not so widely known.

If we are comparing measured amplitudes from a series of events that have similar waveforms and are recorded by the same (nominal) instrument, then the errors 1 - 3 listed above should be normally distributed and can be accounted for by statistical methods. Let us here pose a different question. Assume that the same ground motion is recorded by a number of different instruments and that the measurements are accurately made. After correcting for the instrument response at the apparent period of the cycle being measured, how closely do the estimates of ground motion agree? In this appendix we give the results of several numerical experiments that indicate that the differences can be surprisingly large.

First, let us consider the effect on body wave measurements. The instruments to be discussed are as follows. For the standard of comparison let us take the LRSM Benioff short period instrument for which nominal response curves were given in all the old SDAC shot reports. We have been interested in computing the ground motion at five SDAC stations, RKON, CPSO, WH2YK, FNWV, HNME. Calibration data from June 12, 1975 was supplied by the Project Officer for each of these stations. This was in the form of ≈ 5 amplitude response values and a series of phase response values. The data were not entirely consistent and had to be smoothed. Certainly, it is valid to ask how trustworthy these calibration data are, but they are the best we have. The amplitude response of these six instruments is plotted in Figure A.1.

Let us view the same explosion-like ground motion through the six instruments which we denote as LRSM and by the names of the five SDCS stations. The ground motion is that computed for KASSERI at HNME with T/Q = 1.05. The resulting seismograms are shown in Figure A.2. In terms of signal shape, the main difference is that distinguishing the LRSM record from the other five. We also notice that the 1 Hz peak amplitude values given with each record vary over a substantial range (1.02 - 1.36 μ) with the LRSM record again being exceptional.

What are the amplitudes associated with the seismograms of Figure A.2? With these theoretical records we can reduce the measurement errors to nearly vanishing. Rather than measuring by eye, a parabola is fit to the digital data defining the peaks. The amplitude and apparent period of the cycle of interest can then be determined with sources of human error removed. Since the instrument is input to the code in digital form, we can determine the (theoretical) instrument response at the apparent period with essentially zero error. The amplitude and period data for the b and d phases are summarized in Table A.2. The maximum or d phase is indicated on the seismograms by a bar.

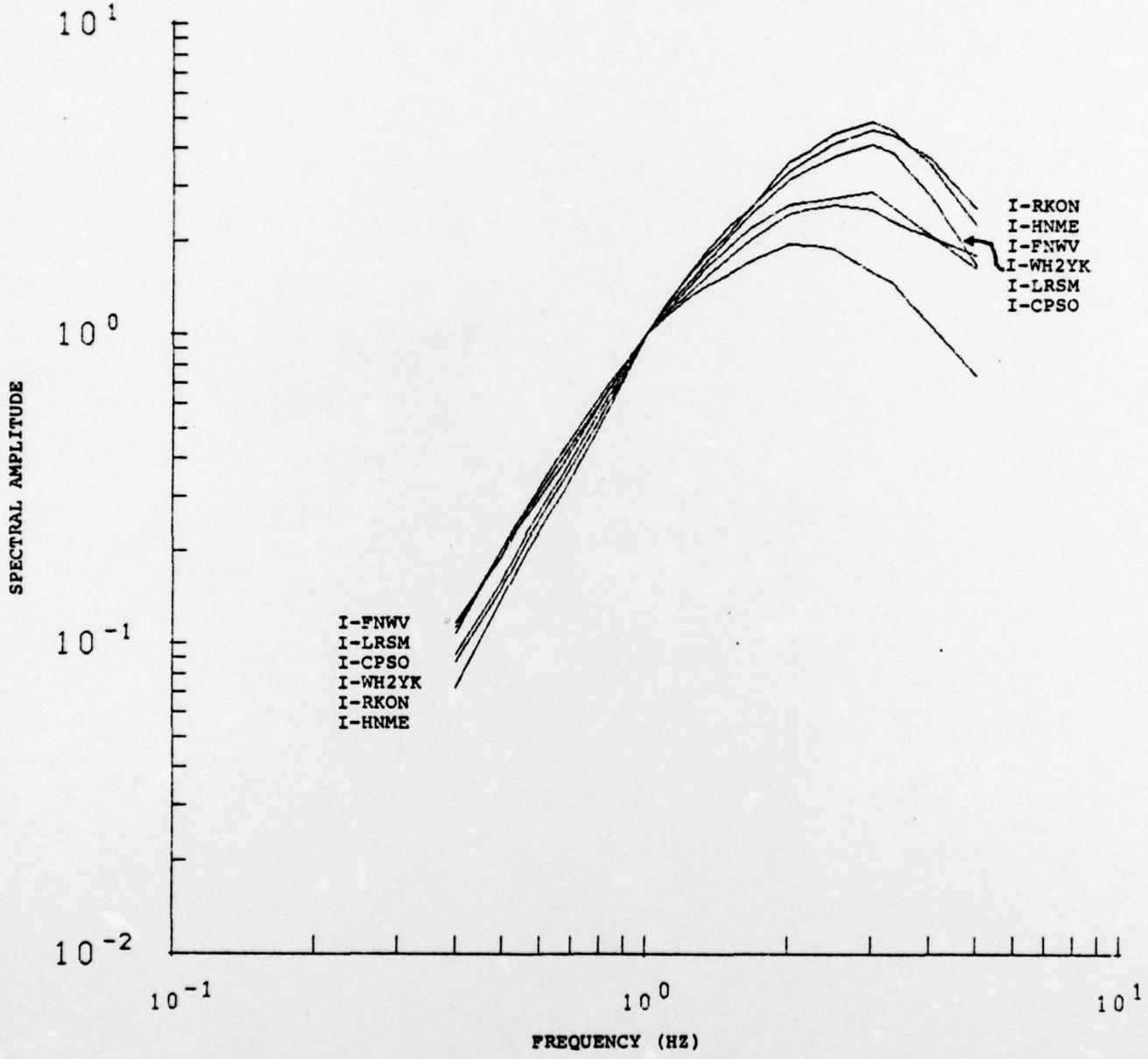

Figure A.1. Amplitude response for six short period instruments. The ordering of the first and last points plotted is indicated.

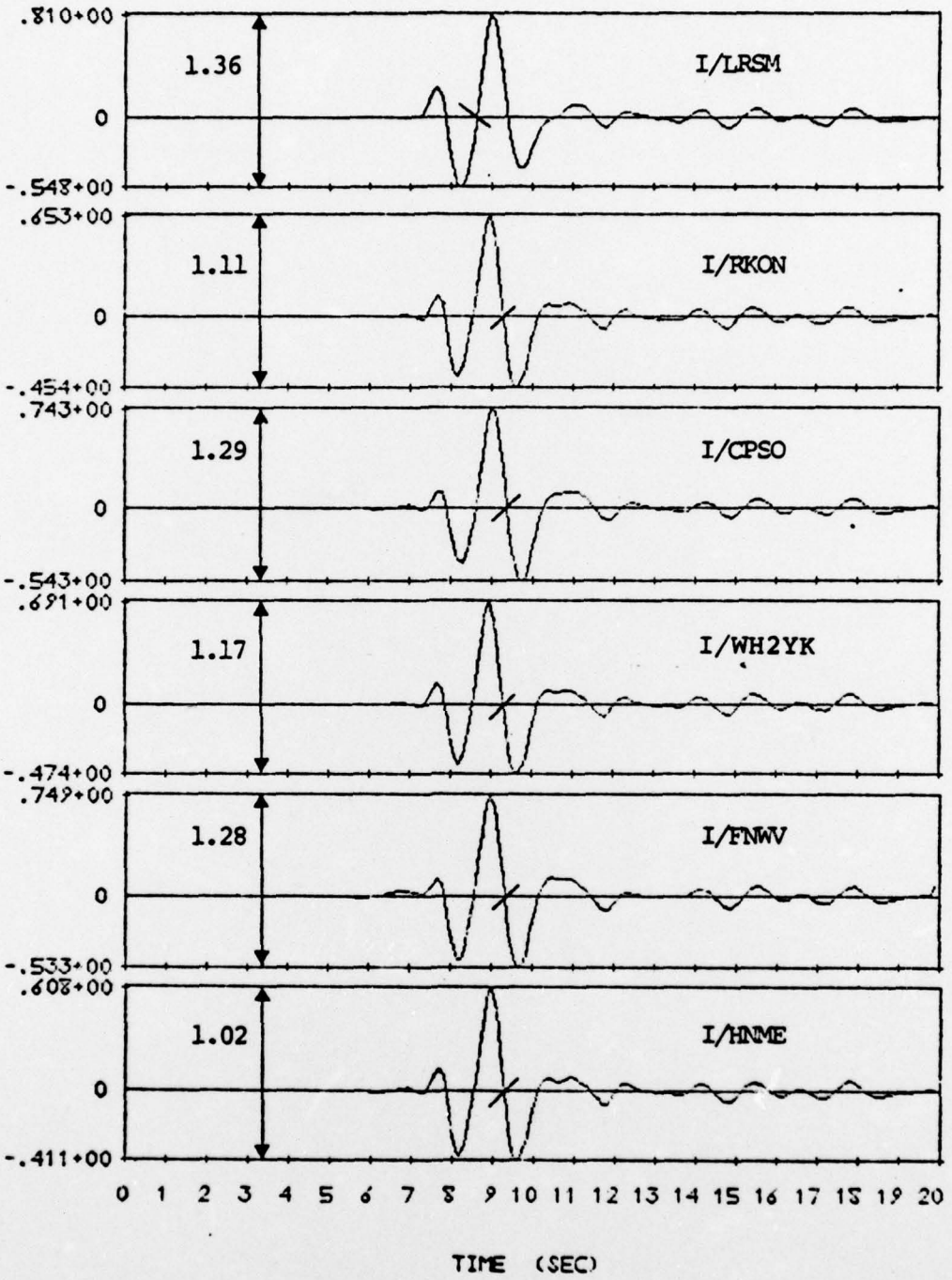

Figure A.2. Theoretical ground motion for KASSERI at HNME as viewed with six different instruments. The instrument designations appear on each seismogram as I/name. For the calculations T/Q = 1.05.

Table A.1. Amplitude and Period Data for the Records of Figure A.2

Instrument	T_b	b (mμ)	T_d	d (mμ)
I/LRSM	1.16	1079	1.52	3373
I/RKON	0.97	493	1.35	2589
I/CPSO	1.05	607	1.43	3093
I/WH2YK	0.99	537	1.37	2670
I/FNWV	1.06	686	1.39	2725
I/HNME	0.97	491	1.32	2390

The amplitude and period differences are startling. If we just consider the SDCS instruments, the period varies by 0.1 second and the amplitude by ≈ 40 percent. However, including the LRSM, the b amplitudes vary by more than a factor of two! Unfortunately, the instrument correction acts in the wrong way. If we were to make no instrument correction other than to the gain at 1 Hz, the discrepancy in amplitudes in the data of Table A.1 would be much reduced. For example, with no correction the b amplitudes for the SDCS instruments vary from 523 - 596 mμ and the LRSM amplitude is 783 mμ. Perhaps we should not make instrument corrections!

What about when the actual ground motion is different from that used in the comparison above? Let us consider KASSERI as computed at each of the SDCS stations with earth model HWNE-3 and T/Q = 1.05. We compute seismograms at each of the stations, first with the LRSM nominal instrument, then the instrument response specific to each station. The results are shown in Figure A.3 and the amplitudes are summarized in Table A.2.

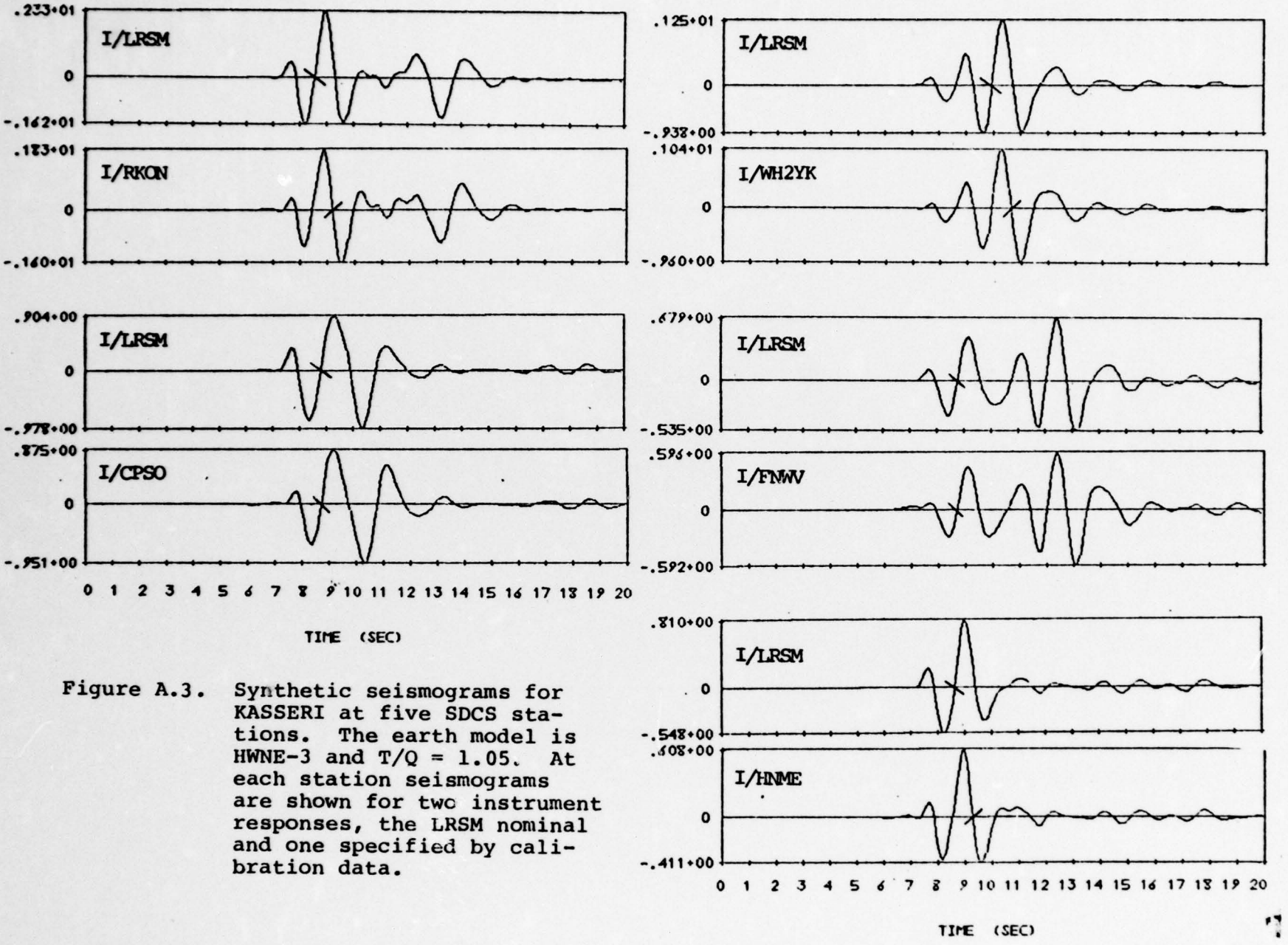

Figure A.3. Synthetic seismograms for KASSERI at five SDCS stations. The earth model is HWNE-3 and T/Q = 1.05. At each station seismograms are shown for two instrument responses, the LRSM nominal and one specified by calibration data.

Table A.2. Amplitude and Period Data for the Records of Figure A.3

Station	Instrument	T_b	b	T_d	d
RKON	LRSM Nominal	1.09	2682	1.48	9345
	Specific	0.95	1337	1.35	2589
CPSO	LRSM Nominal	1.29	2061	1.84	6986
	Specific	1.17	1249	1.43	3093
WH2YK	LRSM Nominal	1.19	646	1.38	4452
	Specific	1.03	336	1.37	2670
FNWV	LRSM Nominal	1.43	1078	1.49	2024
	Specific	1.38	732	1.39	2725
HNME	LRSM Nominal	1.16	1079	1.52	3373
	Specific	0.97	491	1.32	2390

In Table A.3 we show the same kind of comparison for ground motion from the MAST event. In this case the dominant period of the actual ground motion is somewhat shorter than for KASSERI. Only the data for the b amplitude are shown as they illustrate our point — the instrument response can make a big difference in the apparent ground motion determined from seismograms by conventional means.

Table A.3. Amplitude and Period Data for MAST Seismograms Computed with the LRSM Nominal and Station Specific Instruments

Station	Instrument	T_b	b
RKON	LRSM Nominal	0.93	1154
	Specific	0.86	775
CPSO	LRSM Nominal	0.94	603
	Specific	0.92	478
WH2YK	LRSM Nominal	0.94	237
	Specific	0.89	167
FNWV	LRSM Nominal	1.08	248
	Specific	1.02	168
HNME	LRSM Nominal	0.93	415
	Specific	0.86	270